

Characterization of gold nanoparticles modified with single-stranded DNA using analytical ultracentrifugation and dynamic light scattering

James B. Falabella^{1*}, Tae Joon Cho¹, Vincent A. Hackley¹, and Michael J. Tarlov¹

¹National Institute of Standards and Technology

Abstract

We report the characterization of gold nanoparticles modified with thiol-terminated single stranded DNA using analytical ultracentrifugation and dynamic light scattering. Sedimentation coefficients of nominally 10 and 20 nm diameter gold nanoparticles modified with thiol-terminated thymidine homo-oligonucleotides, 5 to 30 bases in length, were determined with analytical ultracentrifugation. The sedimentation coefficients of the gold nanoparticles were found to decrease with increasing coverage of DNA and increasing number of thymidine nucleotides (dT). It was found that sedimentation coefficients for DNA modified gold particles were most closely predicted when the strands were modeled as fully extended chains (FEC). Calculation of apparent particle density from the measured sedimentation coefficient revealed that as the bare particle size decreased a significant hydration layer greatly reduces the apparent density of bare and short DNA chain modified gold particles.

Keywords: gold nanoparticles; ssDNA modified; analytical ultracentrifugation; hydration effects.

* Author to whom correspondence should be addressed.

Introduction

Biologically-modified nanomaterials are being intensely studied and developed for a variety of different biomedical applications. These materials are being considered for use as therapeutic agents, vehicles for targeted drug delivery, and diagnostic probes¹⁻³. In therapeutic applications, these materials are expected to receive intense regulatory scrutiny in order to be approved for use in human subjects. Any nanoparticle-based therapeutic will undergo rigorous characterization using an arsenal of orthogonal methods to assess the critical physical, chemical, and biological attributes that contribute to its efficacy and safety. Among these attributes, particle size distribution and biomolecular surface coverage will likely figure prominently and robust analytical methods will be needed for their assessment.

If a nanoparticle-based therapeutic is coated with biomolecules, the molecular surface loading of each batch will need to be monitored to detect any significant variation that might affect drug efficacy or safety. The conformation of the molecules at the surface of a biologically-modified nanoparticle will also be important because a change in the molecular surface configuration may reduce the accessibility of active sites or possibly lead to aggregation of the particles. The presence of aggregates of particles may be of particular concern because of the possibility of these aggregates being immunogenic, i.e., causing an immune reaction in patients that leads to neutralization of the drug, similar to what has been observed for aggregated protein therapeutics and vaccines^{4,5}. Ensuring a proper size distribution within a batch of biologically modified nanomaterials may also affect drug efficacy and safety because many of these therapies will likely exploit the selectivity in delivery afforded by the relatively larger openings in the walls of blood vessels in the cancerous tissue⁶.

There are several well-established methods for sizing nanomaterials that can also be used to detect their potential aggregation and provide information concerning their surface modification. Among the most widespread are size exclusion chromatography (SEC)^{7,8}, asymmetric field flow fractionation (AFFF)⁹, dynamic light scattering (DLS), and analytical ultracentrifugation (AUC)⁹. Size distributions from DLS alone are non-trivial to obtain without prior knowledge of whether aggregation is occurring⁹. If the particles differ in hydrodynamic diameter by less than several fold, one must employ AFFF to pre classify particles before performing DLS. The membrane unit for performing AFFF dilutes the sample in the process of segregating the particles of different size, which can decrease the measured concentration of aggregates if the particles are not permanently bound together. Krueger et al⁹ recently employed SEC to separate polystyrene stabilized nanoparticles of Au and CdSe in toluene. SEC often requires sample dilution, which can also alter aggregate distributions, and the interaction of the material with the column matrix may further perturb aggregates.

In contrast, analytical ultracentrifugation can examine samples over a wide range of solution conditions and concentrations and detect low levels of aggregated protein therapeutics that cannot be detected with SEC. With sub-nanometer resolution¹⁰, AUC can often classify samples when other analytical methods fail to detect any difference in particle size or molecular surface coverage. Recently, nanoparticles of CdS¹¹, CdSe¹¹, and TiO₂¹² less than 20 nm in diameter were characterized with AUC and differences in sedimentation coefficients were attributed to varying surface texture of the nanoparticles. Machtle et al.¹³ also demonstrated the impressive range of particle sizes that can be measured with AUC by implementing a rotor speed gradient program to classify polystyrene spheres ranging from 20 to 2 000 nm in diameter. AUC of biologically modified nanomaterials was recently reported by Calabretta et al.¹⁴ and Jamison

et al.¹⁵ where they examined the formation of DNA - LacI protein complexes on the surface of 10 nm gold nanoparticles^{14,16,17}. Their study showed that AUC could discern between LacI-modified gold nanoparticles with and without bound DNA. Although these recent investigations demonstrate the ability of AUC to distinguish between nanoparticles of different size and nanoparticles modified with biological molecules, there have been no AUC studies reported that have systematically examined the surface loading or length of biopolymers tethered to nanoparticles, such as single-stranded DNA (ssDNA) oligomers. To fill this gap, we report here the use of AUC to determine sedimentation coefficients of gold nanoparticles nominally 10 and 20 nm in diameter that are modified with thiol-terminated single-stranded thymine homooligomers from 5 to 30 bases in length. We compare the sedimentation coefficients determined using AUC for these materials with models that provide insight into the conformation of molecules at the particle surface.

Experimental *

Chemicals

The nominally 10 nm diameter gold nanoparticles used in this study were National Institute of Standards and Technology (NIST) Reference Material 8011¹⁸. Other NIST reference materials used in this study are nominal 30 and 60 nm diameter gold nanoparticles (NIST RM 8012¹⁹ and 8013²⁰). This NIST reference material consists of citrate-stabilized gold nanoparticles suspended in water. The dimensions of these nanoparticles were measured by NIST using six independent methods—atomic force microscopy (AFM), transmission electron microscopy (TEM), scanning electron microscopy (SEM), electro spray-differential mobility analysis (ESDMA), dynamic light scattering (DLS), and small-angle X-ray scattering (SAXS)—and these results are reported in the NIST Report of Investigation¹⁸. The nominally 5 and 20 nm diameter

gold nanoparticles were purchased from Ted Pella (Redding, CA) and sized using ES-DMA in our laboratory according to the method of Pease et al.²¹. The nanoparticles purchased from Ted Pella are electron microscopy grade with nominal particle concentrations of 5.0×10^{13} particles ml^{-1} (5 nm diameter) and 7×10^{11} particles ml^{-1} (20 nm diameter). Thymidine homo-oligomers were purchased from Integrated DNA Technologies (Coral, IA) with a 3' dithiol modification of the general formula $\text{HO}(\text{CH}_2)_3\text{-S-S-}(\text{CH}_2)_3\text{-T}_x$ (where subscript x is the number of bases which varies from 5 to 30) were used for all ssDNA-gold conjugates. NaCl (99.999 % pure) and MgCl_2 were purchased from Aldrich (Milwaukee, WI) and used as received. Thymidine homo-oligomers in four different lengths including 5, 10, 20, and 30 bases were purchased to examine the effect of increasing ssDNA strand length. Ultra pure 18 M Ω water from a Barnstead Nanopure UV water purifier (Beverly, MA) was used for preparing solutions for all experiments.

Procedure for preparing gold nanoparticle-ssDNA homo-oligomer conjugates

Thiolated thymidine homo-oligomers were first dissolved in deionized water to a concentration of $200 \mu\text{mol L}^{-1}$. To prepare the ssDNA – gold conjugates $6 \mu\text{L}$ of ssDNA stock solution was added to $100 \mu\text{L}$ of gold nanoparticles as received from the vendor. The ssDNA and gold nanoparticles were mixed by vortexing for 2 s and then allowed to sit at room temperature (21 C) for 18 h. A concentrated 5.5 mol L^{-1} NaCl solution was added to bring the total salt concentration to a first step of 0.11 mol L^{-1} . The mixture was vortexed and allowed to sit at room temperature for 3 h before adding an additional volume of concentrated NaCl solution to raise the final NaCl concentration with the purpose of increasing the ssDNA loading on the particles. Final NaCl concentrations used for this study were 0.80, 1.52, and 2.41 mol L^{-1} with ssDNA concentrations decreasing from 11 to $6 \mu\text{mol L}^{-1}$ as the salt concentration increased. It was estimated that the concentration of the ssDNA in solution was a factor of ten or greater in

excess of the concentration needed to result in full monolayer coverage for gold nanoparticles assuming that saturation coverage is $\approx 2.5 \times 10^{13}$ strands cm^{-2} as determined by Demers et al.²². After the desired final salt concentration was achieved, the mixture was allowed to sit for 48 h at room temperature. The ssDNA-modified particles were then pelleted in their holding tubes using a Beckman Coulter (Fullerton, CA) Optima Max-XP bench top ultracentrifuge outfitted with a MLA-50 swinging bucket rotor outfitted with Beckman Coulter Konical™ vials at a rotational speed of $2\,260 \text{ rad s}^{-1}$ (21 600 rpm) for 15 min. All but 20 μL of the supernatant was withdrawn and the pellet of nanoparticles was replaced with an equal volume of deionized water and the ssDNA-gold particles were completely re-suspended by vortexing for 2 s.

Dynamic light scattering

A Malvern Zetasizer Nano (Worcestershire, UK) was used to perform dynamic light scattering at a 3 rad (173 degree) backscattering angle for samples 100 μL in volume. For these experiments, samples of DNA-modified gold nanoparticles were recovered from the AUC cells and filtered through a $4.5 \times 10^{-7} \text{ m}$ (0.45 μm) polyvinyl difluoride membrane filters (Daigger, Vernon Hills, IL) to remove dust.

Analytical Ultracentrifugation

Analytical ultracentrifugation of all samples was performed using a Beckman Coulter XL-A with a titanium 4 place rotor (Beckman Coulter). Cells were outfitted with quartz windows and Epon™ 12 mm path length dual sector centerpieces and quartz windows. The reference sector of each cell was filled with 425 μL of deionized water while the sample sector was filled with 400 μL of modified or unmodified gold nanoparticles suspended in deionized water. All samples were diluted to the same final concentration of particles per milliliter to eliminate concentration effects. Absorbance was measured at a wavelength of 520 nm at scan intervals of

0.007 cm. Gold nanoparticles 5 and 10 nm in diameter were centrifuged at $1\,570\text{ rad s}^{-1}$ (15 000 rpm) and 20 nm gold nanoparticles were centrifuged at 523 rad s^{-1} (5 000 rpm). Bare gold nanoparticles 30 and 60 nm in diameter were centrifuged at 262 rad s^{-1} (2,500 rpm). All AUC runs were performed at $20\text{ }^{\circ}\text{C}$. The optimal rotor speed was determined experimentally by examining a range of rotor speeds and using the slowest possible speed allowing the sedimentation front to be scanned at least 10 times at intervals of 130 s before the nanoparticles completely pelleted at the bottom of the cell.

Results and Discussion

Biologically modified gold particles

Raw sedimentation velocity data from multiple scans of a cell containing unmodified, citrate-stabilized 10 nm gold nanoparticles are displayed in Figure 1. These data are typical for all gold nanoparticle sample solutions examined in this study. Modification of gold nanoparticles with thymidine homo-oligonucleotides was selected for our studies because this system has been extensively studied on planar gold surfaces where it has been established that thymidine bases have a relatively low affinity for gold surfaces²³ and base-pairing interactions are weak²⁴. These factors tend to favor relatively high surface coverages and an upright configuration for thiol-modified thymine strands attached to gold surfaces. Sedimentation of the 10 nm gold nanoparticles was carried out in both pure water and 1 mol L^{-1} solutions of NaCl and MgCl_2 .

Sedimentation coefficients were calculated from the raw data using Sedfit by Schuck²⁵. Sedfit numerically fits the Lamm Equation to the complete set of 520 nm wavelength absorbance scans of each sample cell shown in Figure 1. Representative sedimentation coefficient distributions for bare 10 nm gold particles and 10 nm particles with increasingly longer ssDNA strands from 5 to 30 bases in length are displayed in Figure 2. These data have several

noteworthy features. First, modification of nanoparticles with DNA reduces their sedimentation coefficient. Second, as the length of DNA increases, the sedimentation coefficient distribution moves monotonically to lower values. We believe that the small shoulder in the sedimentation coefficient distributions for SH-T10 and SH-T20 was aggregates that were not broken up by the attachment of ssDNA. The narrower sedimentation coefficient distributions for the ssDNA modified 10 nm gold NPs in Figure 2 suggest that the bonding of the thiolated ssDNA reduces the number of aggregates in a sample. Aggregates of bare gold NPs have also been observed by Pease et al.²¹ using electrospray differential mobility analysis (ES-DMA). Weight average sedimentation coefficients were calculated using the integrate feature of Sedfit²⁵ and these values are plotted in Figure 3 for the 10 nm ssDNA modified particles as a function of ssDNA length in pure water and 1 mol L⁻¹ NaCl and MgCl₂ solutions.

The sedimentation coefficients for the DNA-modified gold nanoparticles decreases monotonically with number of thymidine, dT, nucleotides or strand length. We note that the reproducibility of the sedimentation coefficients is excellent as evidenced by the small standard deviations derived from 3 measurements. The sedimentation coefficients for 10 nm nanoparticles derivatized with dT 5- and 10-mers were not measured in 1 mol L⁻¹ MgCl₂ because significant flocculation occurred in these solutions. In addition, the sedimentation coefficients of gold nanoparticles with dT 20- and 30-mers in pure water appear to be slightly lower than those sedimented in 1 mol L⁻¹ salt solution suggesting that the hydrodynamic diameter of these particles is smaller in salt solution. This behavior suggests that the DNA strands on the particle's surface assume a more compact configuration consistent with the persistence length of the ssDNA strands decreasing with salt concentration²⁴. The sedimentation coefficients of ssDNA gold particles centrifuged with either dissolved Mg²⁺ or Na⁺ ions were identical.

Detecting differences in ssDNA surface coverage with AUC

We also found that AUC can detect differences in surface coverage of ssDNA homooligomers on gold nanoparticles. Analytical ultracentrifugation has been able to distinguish sub-nanometer size differences in solid particles^{26,27}. To vary the surface coverage of ssDNA on gold nanoparticles, different batches of thymine-modified 10 nm gold nanoparticles were prepared with systematically higher ending NaCl concentrations to progressively increase the surface loading of ssDNA. In these experiments, all samples were resuspended in pure deionized water before sedimentation in the AUC. Figure 4 demonstrates that an increase in ssDNA surface coverage (more salt added during the attachment phase to promote more ssDNA attachment on the gold nanoparticle)²⁸ leads to a slight, but significant, decrease in the weight average sedimentation coefficient. This result is expected because the addition of more ssDNA will lead to a decrease in the apparent density of the gold nanoparticle.

Particle models

Two models were developed to provide greater insight into the experimental trends in sedimentation coefficients as a function of the length of the ssDNA. The first model illustrated in Figure 5a treats the derivatized particle as having fully extended chain (FEC) dT strands tethered to the particles in a hexagonal close packed formation. Although it is unlikely that the ssDNA strands are hexagonally close packed on the nanoparticle surface, we believe this assumption is reasonable because only a weak dependence of ssDNA coverage on the sedimentation coefficient is observed in Figure 3. The second model illustrated in Figure 5b treats each dT strand as a worm like chain (WLC) that is coiled randomly about its thiol tether. The overall density of the bare or ssDNA-modified particle is calculated by the general relationship:

$$\rho_2 = \frac{M_{DNA} + M_p + M_w}{V_{DNA} + V_{particle} + V_w} \quad (1)$$

Where ρ_2 is the density of the bare or ssDNA modified particle, M_{DNA} is the total mass of ssDNA attached to the particle, M_p is the mass of the gold particle, and M_w is the mass of the water hydrating the chains of ssDNA. The total volume of the particle consists of the sum of the volumes of the gold particle ($V_{particle}$), the DNA molecules (V_{DNA}), and the water confined between ssDNA chains (V_w).

The FEC ssDNA model is illustrated in Figure 5a with water of hydration filling the space between the ssDNA chains. Each chain of ssDNA extends normal to the surface and a dry cylindrical envelope surrounding the chain is used to prevent the model from placing water in the same space as the ssDNA chain. The relationship for calculating the overall density for a bare or ssDNA modified gold nanoparticle, the FEC model is as follows:

$$\rho_2 = \frac{m_{DNA}n_{DNA}}{4/3\pi(r_p + l_{DNA})^3} + \frac{\rho_p r_p^3 + \rho_w (r_p + l_{DNA})^3 - \rho_w r_p^3}{(r_p + l_{DNA})^3} - \frac{\rho_w l_{DNA} r_{envelope}^2}{1/3(r_p + l_{DNA})^3} \quad (2)$$

Where m_{DNA} is the mass of one ssDNA chain, n_{DNA} is the number of ssDNA chains on one gold NP, l_{DNA} is the length of one DNA chain, ρ_p is the density of the gold NP, r_p is the radius of the gold NP, $r_{envelope}$ is the radius of a dry cylindrical envelope surrounding the fully extended chain, and ρ_w is the density of liquid water between chains of ssDNA. The length of the fully extended ssDNA and the volume of the dry envelope around each chain are calculated using an individual dT length of 0.59 nm²¹. This model was used to predict only sedimentation coefficients in pure water therefore the density of the water between ssDNA molecules was assumed to be the density of bulk water at 20 C or 998.23 kg m⁻³. While the density of water in confined spaces may be different from bulk water, the difference is likely insignificant to the numerical result. The density of gold nanoparticles is assumed to be that of bulk gold (19 300 kg m⁻³) based on the

finding of Li et al.²⁹ that gold clusters as small as 20 atoms have the same atomic packing as bulk gold. For these calculations, we consider the ssDNA adsorbed on the surface of the nanoparticles to be hexagonally close packed. We note again that this assumption is a simplification and it is unlikely that adsorbed chains possess any long-range order on the nanoparticle surface.

With the density of the modified gold nanoparticle calculated by the model, the sedimentation coefficients of the biologically modified gold particle are calculated with an expression based on the Svedberg relationship:

$$\frac{s}{D} = \frac{M(1 - \bar{v}_2\rho_1)}{RT} \quad (3)$$

where s is the sedimentation coefficient of the ssDNA-modified unit, D is the diffusion coefficient of the particle, M is its molecular weight, R is the gas constant, T is the sample temperature, ρ_1 is the matrix fluid density, and \bar{v}_2 is the partial specific volume of the nanoparticle. Since the gold nanoparticles are a dilute suspension, D can be replaced with the following two relationships:

$$f = \frac{RT}{ND} \quad (4)$$

$$f = 6\pi\eta_1R_s \quad (5)$$

where f is the particle's friction factor, N is Avogadro's number, η_1 is the viscosity of the matrix fluid, and R_s is the radius of a spherical nanoparticle. The mass of a mole of the hydrated modified nanoparticles, M , is substituted with the following expression:

$$M = \frac{4\pi NR_s^3}{3\bar{v}_2} \quad (6)$$

Equations 3 to 6 are then combined to obtain Eq 7:

$$s = \frac{2R_s^2(1 - \bar{v}_2\rho_1)}{9v_2\eta_1} \quad (7)$$

Substituting density for the partial specific volume of the modified nanoparticle, $\bar{v}_2 = 1/\rho_2$, yields an expression for the sedimentation coefficient of a biologically modified nanoparticle in terms of,

$$s = \frac{2R_s^2(\rho_2 - \rho_1)}{9\eta_1} \quad (8)$$

where ρ_2 is the density of the hydrated ssDNA-modified nanoparticle.

A comparison of FEC model predictions with experimentally determined sedimentation coefficients is plotted in Figure 6. The FEC model predictions had an absolute average deviation (AAD) from the measured sedimentation coefficients of $\approx 60\%$ for 10 nm gold nanoparticles and $\approx 25\%$ for 20 nm gold nanoparticles. Reasonable agreement between the measured sedimentation coefficients and the FEC predictions is found for 20 nm gold nanoparticles modified with 20, and 30 dT chains.

Worm like chain model

Since ssDNA chains more likely adopt a random coil configuration, the worm like chain (WLC) model³⁰ was used to calculate the radius of the hemispherical ssDNA coils on the surface of the gold particle. A particle representing the WLC model is illustrated in Figure 5b. Each end-tethered ssDNA molecule is confined to a dry hemispherical envelope to prevent water from occupying the same space as the ssDNA and the envelopes are again assumed to arrange in hexagonal close packing on the gold surface. The WLC model for polymer chains is selected because it has been previously used to model the end-to-end distance of single and double stranded DNA²⁴. The WLC model for polymer chains requires just two parameters: the fully

extended length of the ssDNA chain and the persistence length to model the stiffness of the molecule. These two parameters are related as:

$$\langle R^2 \rangle = 2l_p R_{max} - 2l_p^2 \left(1 - \exp\left(-\frac{R_{max}}{l_p}\right) \right) \quad (9)$$

where $\langle R^2 \rangle$ is the end-to-end distance of the ssDNA chain, R_{max} is the length of a fully extended ssDNA chain, and l_p is the persistence length of a ssDNA chain. Values of R_{max} and l_p for both the 10 and 20 nm ssDNA modified gold nanoparticles are contained in Table 2. A value of 2.5 nm is used for the persistence length of thymine homo-oligomers in pure water as reported by Murphy et al.²⁴. The R_{max} varied from approximately 3 to 18 nm based on a 0.59 nm length for each base. The relationship for the overall density of bare or ssDNA modified gold nanoparticles is as follows:

$$\rho_2 = \frac{m_{DNA}n_{DNA}}{4/3\pi(r_p + \langle R^2 \rangle)^3} + \frac{\rho_p r_p^3 + \rho_w (r_p + \langle R^2 \rangle)^3 - \rho_w r_p^3 - \rho_w \langle R^2 \rangle^3 / 2}{(r_p + \langle R^2 \rangle)^3} \quad (10)$$

Predictions of measured sedimentation coefficients by the WLC model assuming a gold core density (ρ_p) of 19 300 kg m⁻³ are shown in Figure 6. The WLC model predictions are likely higher than those of the FEC model because the thickness of the coiled ssDNA layer is less than the layer of fully extended ssDNA and hence the average density of the gold and ssDNA shell is lower when the ssDNA shell is thicker. As a result, the WLC model provides poorer agreement than the FEC model, most notably at longer strand lengths, with absolute average deviations (AAD) of $\approx 70\%$ for 10 nm gold nanoparticles and $\approx 30\%$ for 20 nm gold nanoparticles.

Dynamic light scattering was performed to determine whether the WLC or FEC model predicted the diameter of the particles more accurately. Figure 7 plots the measured hydrodynamic diameter of bare and ssDNA modified gold nanoparticles in pure water along with diameter

predictions from both the WLC and FEC models., The FEC model overestimates the measured hydrodynamic diameters for strands greater than 5 bases in length, while the WLC model predictions follow the measured diameters more closely. Thus, the poorer sedimentation coefficient predictions by the WLC model shown in Figure 6 are most likely due to the predicted particle density being higher than the apparent particle density. This could be caused by a hydration layer that is not detected by DLS, however the density difference causes a clear difference between model and data when predicting the sedimentation coefficient of bare and ssDNA modified gold nanoparticles.

To illustrate the degree to which the apparent density of bare gold nanoparticles varies with the particle diameter in pure water, sedimentation velocity experiments were performed on bare gold nanoparticles with nominal diameters from 5 to 60 nm listed in Table 1. Equation 8 was used to calculate the apparent density of the bare particles, ρ_2 , from the measured sedimentation coefficient and measured particle diameter as determined with electrospray differential ion mobility analysis (ES-DMA)²¹. Figure 8, which plots the apparent particle density from AUC versus the measured particle diameter, demonstrates that the hydration of the gold nanoparticle significantly lowers the calculated density of bare gold nanoparticles.

Nanoparticles in the range of 60 nm and above appear to obey the Svedberg equation and their apparent density approaches that of bulk gold (19 300 kg m⁻³). This hydration effect for sub 60 nm gold nanoparticles may also affect the gold nanoparticles with the shortest length ssDNA homo-oligomers if the ssDNA cannot completely block water molecules from interacting with the gold surface. Replacing the bulk density of gold with the apparent density shifts the model predictions lower and does not change the steepness of the plots of predicted sedimentation coefficients for 10 and 20 nm gold particles.

Conclusions

The use of biologically modified nanomaterials for biomedical applications in humans will face many regulatory hurdles that can be addressed in part by robust characterization techniques. This paper demonstrates that changes in length of thymidine homooligomer chains immobilized on nanoparticle surfaces can be detected by analytical ultracentrifugation along with differences in molecular surface loading. Prediction of the sedimentation coefficients from first principle models for bare and ssDNA modified gold nanoparticles was not entirely possible due to the hydration effects that reduce the particle's density in an aqueous medium. The hydrodynamic diameters measured with DLS were matched well by the WLC model using the same parameters, revealing that the WLC model will determine a plausible overall diameter for the ssDNA modified gold NP and the reason for the WLC model's poor sedimentation coefficient prediction from first principles indicates possibly a hydration layer of unknown thickness around the particle. This layer of hydration is significant for gold nanoparticles below 60 nm in diameter. Gold nanoparticles 60 nm and higher should approach that of bulk gold ($19\,300\text{ kg m}^{-3}$). The difference between the WLC and FEC models and the measured sedimentation coefficients increases as the ssDNA chain length is reduced. Future modeling must focus on the effect of hydration to adequately predict the sedimentation coefficient of biologically modified gold nanoparticles. Overall, the precision of AUC makes it a well-suited analytical method to perform quality control tests of biologically modified nanomaterials for biomedical applications.

Acknowledgments

We thank Edward Eisenstein of the Center for Advanced Research in Biotechnology for allowing us access to the AUC and Walter Stafford of the Boston Biotechnology Research Institute for useful advice on AUC and modeling the sedimentation coefficient of nanomaterials.

We also thank Suvajyoti Guha for measuring the diameters of two sizes of bare gold nanoparticles and Professor Michael Zachariah for the use of his electrospray differential mobility instrument. J.B.F. thanks the National Research Council for his postdoctoral research fellowship.

***Disclaimer**

The identification of commercial equipment, instruments, or materials in this report is done to adequately describe experimental procedures and does not imply recommendation or endorsement by the National Institute of Standards and Technology.

References

1. Talley, C.E.; Jackson, J.B.; Oubre, C.; Grady, N.K.; Hollars, C.W.; Lane, S.M.; Huser, T.R.; Nordlander, P.; Halas, N.J. *Nano Lett.* **2005**, *5*, 1569.
2. Corrigan, T.D.; Guo, S.; Phaneuf, R.J.; Szmecinski, H. *J. Fluoresc.* **2005**, *15*, 777.
3. Corrigan, T.D.; Guo, S.-H.; Szmecinski, H.; Phaneuf, R.J. *Appl. Phys. Lett.* **2006**, *88*, 101112-101112/3.
4. Cedervall, T.; Lynch, I.; Lindman, S.; Berggard, T.; Thulin, E.; Nilsson, H.; Dawson, K.A.; Linse, S. *Proc. Natl. Acad. Sci. U. S. A.* **2007**, *104*, 2050.
5. Clausi, A.L.; Morin, A.; Carpenter, J.F.; Randolph, T.W. Influence of protein conformation and adjuvant aggregation on the effectiveness of aluminum hydroxide adjuvant in a model alkaline phosphatase vaccine. *J Pharm Sci* **2009**, *98* (1), 114-21.
6. Balogh, L.; Nigavekar, S.S.; Nair, B.M.; Lesniak, W.; Zhang, C.; Sung, L.Y.; Kariapper, M.S.T.; El-Jawahri, A.; Llanes, M.; Bolton, B.; Mamou, F.; Tan, W.; Hutson, A.; Minc, L.; Khan, M.K. *Nanomedicine* *3*, 281.
7. Krueger, K.M.; Al-Somali, A.M.; Mejia, M.; Colvin, V.L. *Nanotechnology* **2007**, *18*, 475709-475709/7.
8. Krueger, K.M.; Al-Somali, A.M.; Colvin, V.L. *Abstracts of Papers, 231st ACS National Meeting, Atlanta, GA, United States, March 26-30, 2006* **2006**, INOR-705.
9. Liu, J.; Andya, J.D.; Shire, S.J. *AAPS J.* **2006**, *8*, E580-E589.
10. Coelfen, H.; Voelkel, A. *Prog. Colloid Polym. Sci.* **2004**, *127*, 31.
11. Mayya, K.S.; Schoeler, B.; Caruso, F. *Advanced Functional Materials* **2003**, *13*, 183.
12. Dollefeld, H.; McGinley, C.; Almousalami, S.; Moller, T.; Weller, H.; Eychmuller, A. *J. Chem. Phys.* **2002**, *117*, 8953.

13. Machtle, W. *Biophys. J.* **1999**, 76, 1080.
14. Calabretta, M.K.; Matthews, K.S.; Colvin, V.L. *Bioconjugate Chem.* **2006**, 17, 1156.
15. Jamison, J.A.; Krueger, K.M.; Yavuz, C.T.; Mayo, J.T.; LeCrone, D.; Redden, J.J.; Colvin, V.L. *ACS Nano* **2008**, 2, 311.
16. Jamison, J.A.; Colvin, V.L. *Abstracts of Papers, 232nd ACS National Meeting, San Francisco, CA, United States, Sept. 10-14, 2006* **2006**, INOR-753.
17. Calabretta, M.K.; Jamison Jennifer A; Falkner Joshua C; Liu Yunping; Yuhas Benjamin D; Matthews Kathleen S; Colvin Vicki L *Nano Lett* 5, 963.
18. Kaiser, D.L.; Watters, R.L. Reference Material 8011 Gold Nanoparticles, Nominal 10 nm Diameter. 2007, https://srmors.nist.gov/reports/view_cert2gif.cfm?certificate=8011.
19. Kaiser, D.L.; Watters, R.L. Reference Material 8012 Gold Nanoparticles, Nominal 30 nm Diameter. 2007, https://srmors.nist.gov/reports/view_cert2gif.cfm?certificate=8012.
20. Kaiser, D.L.; Watters, R.L. Reference Material 8013 Gold Nanoparticles, Nominal 60 nm Diameter. 2007, https://srmors.nist.gov/reports/view_cert2gif.cfm?certificate=8013.
21. Pease, L.F.; Tsai, D.-H.; Zangmeister, R.A.; Zachariah, M.R.; Tarlov, M.J. *J. Phys. Chem. C* **2007**, 111, 17155.
22. Demers, L.M.; Mirkin, C.A.; Mucic, R.C.; Reynolds, R.A.; Letsinger, R.L.; Elghanian, R.; Viswanadham, G. *Anal. Chem.* **2000**, 72, 5535.
23. Kimura-Suda, H.; Petrovykh, D.Y.; Tarlov, M.J.; Whitman, L.J. *J. Am. Chem. Soc.* **2003**, 125, 9014.
24. Murphy, M.C.; Rasnik, I.; Cheng, W.; Lohman, T.M.; Ha, T. *Biophys. J.* **2004**, 86, 2530.
25. Schuck, P. *Biophys. J.* **2000**, 78, 1606.
26. Cölfen, H. ; Pauck, T. *Colloid Polym. Sci.* **1997**, 275, 175.

27. Cölfen, Helmut; Analytical ultracentrifugation of nanoparticles. Anonymous. 2002; PMSE-013.
28. Petrovykh, D.Y.; Kimura-Suda, H.; Whitman, L.J.; Tarlov, M.J. *J. Am. Chem. Soc.* **2003**, *125*, 5219.
29. Li, J.; Li, X.; Zhai, H.-J.; Wang, L.-S. *Science (Washington, DC, U. S.)* **2003**, *299*, 864.
30. Rubenstein, M.; Colby, R.H. *Polymer Physics*; Oxford University Press: New York, NY, 2003.

List of Symbols

D Diffusion coefficient

f Friction factor

l_p Persistence length

l_{DNA} Length of a fully extended ssDNA strand

M Molar mass of the particle

M_{DNA} Mass of attached ssDNA

M_p Total mass of the NP

M_w Total mass of water between DNA strands

m_{DNA} Mass of one ssDNA strand

n_{DNA} Number of DNA strands on a gold nanoparticle

N Avogadro's #

R Gas constant

R_s Hydrodynamic particle radius

R_{max} Fully extended polymer chain backbone length

$\langle R^2 \rangle$ Mean square end-to-end distance

r_p Radius of the gold particle

$r_{envelope}$ radius of the dry envelope around fully extended DNA molecules

s Svedberg coefficient

T System temperature

V_{DNA} Total volume of DNA strands on the particle surface

V_w Total volume of water on the particle surface

$V_{particle}$ Total volume of the gold particle

List of Subscripts

- 1 Matrix fluid
- 2 Particle
- s Spherical

Greek Symbols

- η_1 Viscosity of matrix fluid
- ρ_1 Density of matrix fluid
- ρ_2 Density of the particle
- ρ_w Density of water
- \bar{v}_2 Partial specific volume of the particle

Tables

Table 1. Bare particle sizes.

Nominal particle size / nm	Measured particle size / nm	References
5	8.45	
10	11.3 ^a	18
20	20.3	
30	28.4 ^a	19
60	56.3 ^a	20

^aES-DMA measurement only

Table 2. Parameters of Eq. 9.

Nominal Particle size / nm	# bases per homo-oligomer	R_{max} / nm	l_p / nm
10	5	2.95	2.5
10	10	5.90	2.5
10	20	18.8	2.5
10	30	17.7	2.5
20	5	2.95	2.5
20	10	5.90	2.5
20	20	18.8	2.5
20	30	17.7	2.5

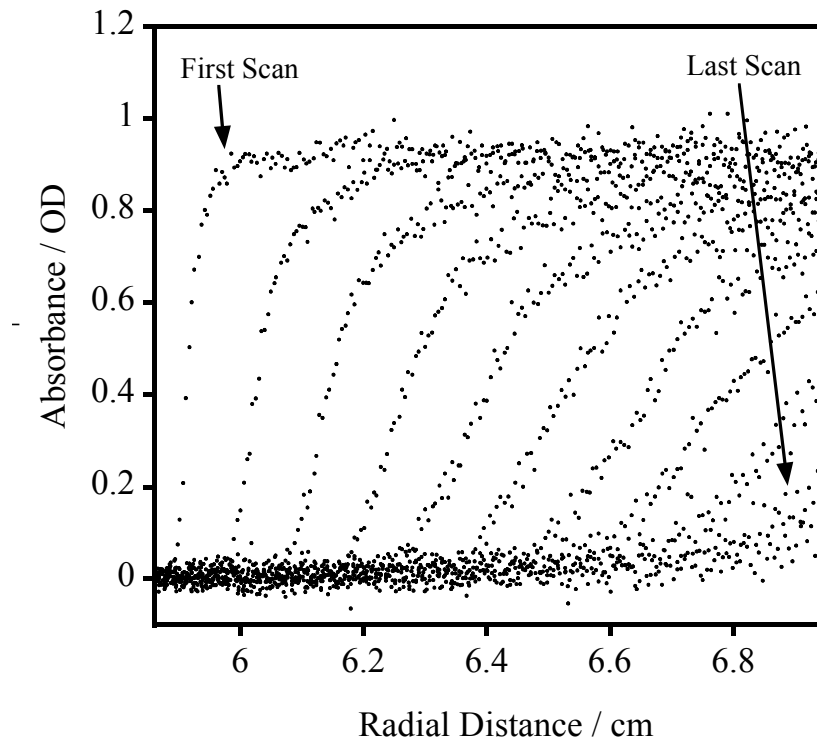


Figure 1. AUC scans for unmodified 10 nm diameter gold nanoparticles centrifuged $1\,570\text{ rad s}^{-1}$ (15,000 rpm). The position of each scan is measured in centimeters from the center of the rotor. Successive scans were taken 130 s apart.

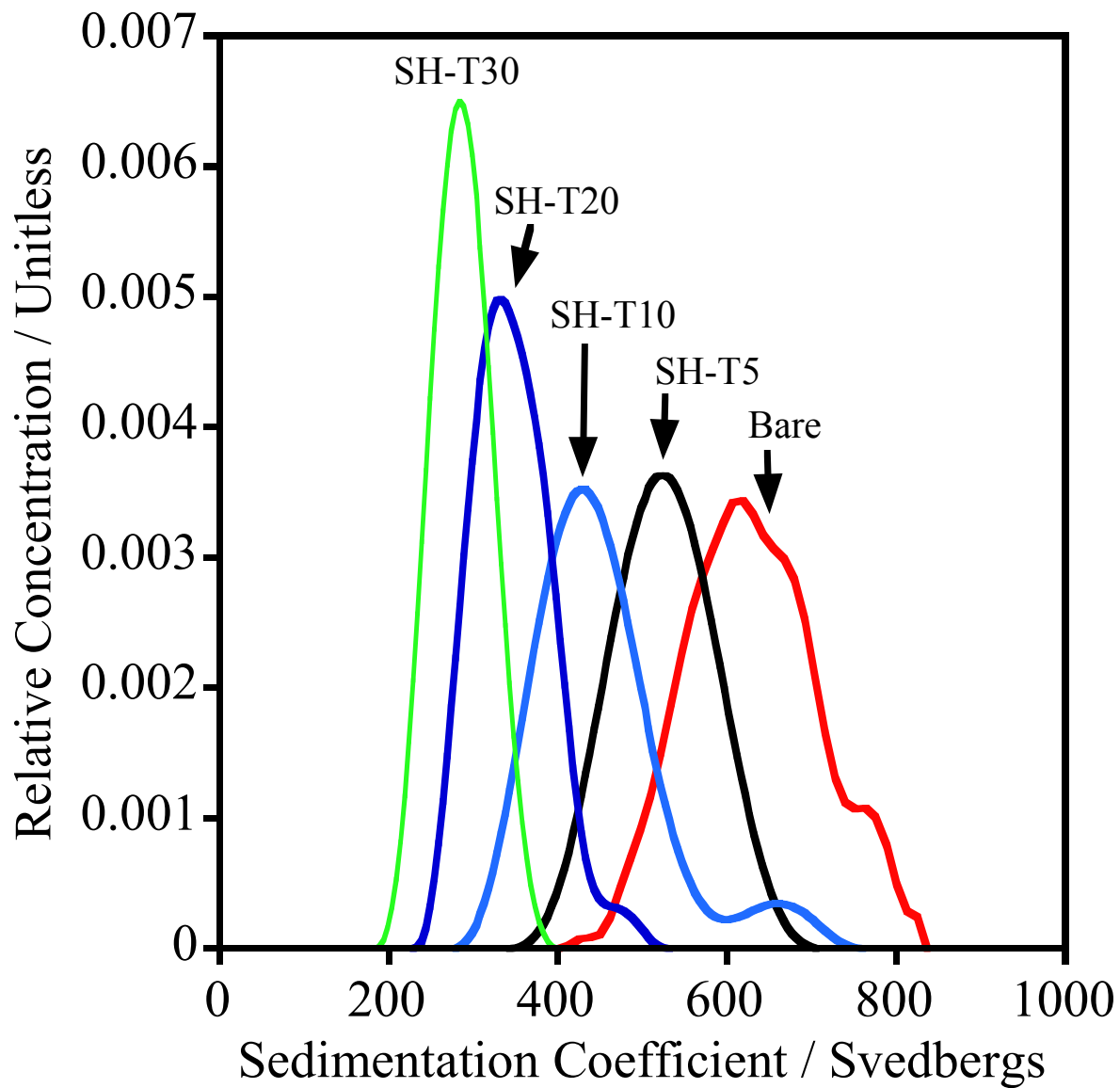


Figure 2: Progression of the sedimentation coefficient distribution for bare 10 nm gold particles and 10 nm gold particles with thymidine homooligomers 30 bases (SH-T30) to 5 bases (SH-T5).

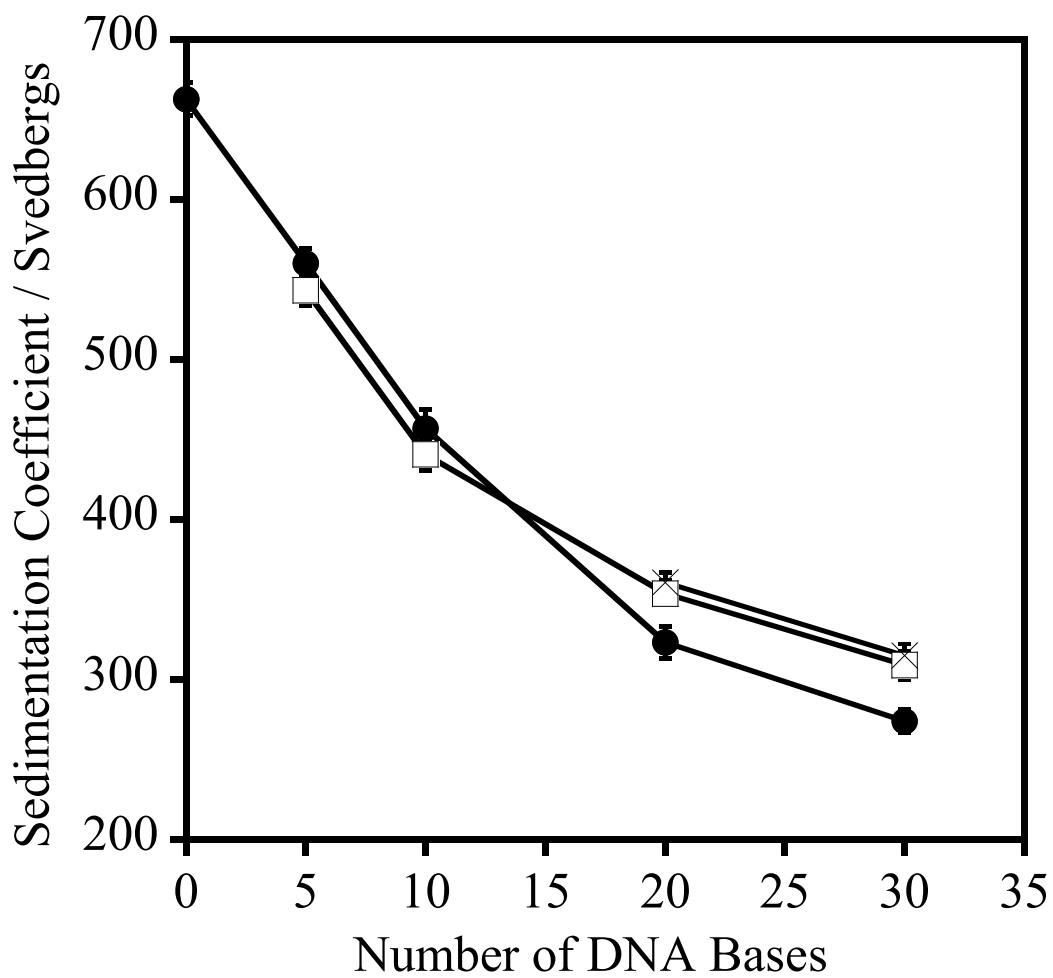


Figure 3. Sedimentation coefficients for 10 nm diameter gold nanoparticles with ssDNA of varying number of dT bases in (●) pure water, (□) 1.0 mol L⁻¹ aqueous NaCl solution, and (×) 1.0 mol L⁻¹ aqueous MgCl₂ solution. Error bars represent standard deviations.

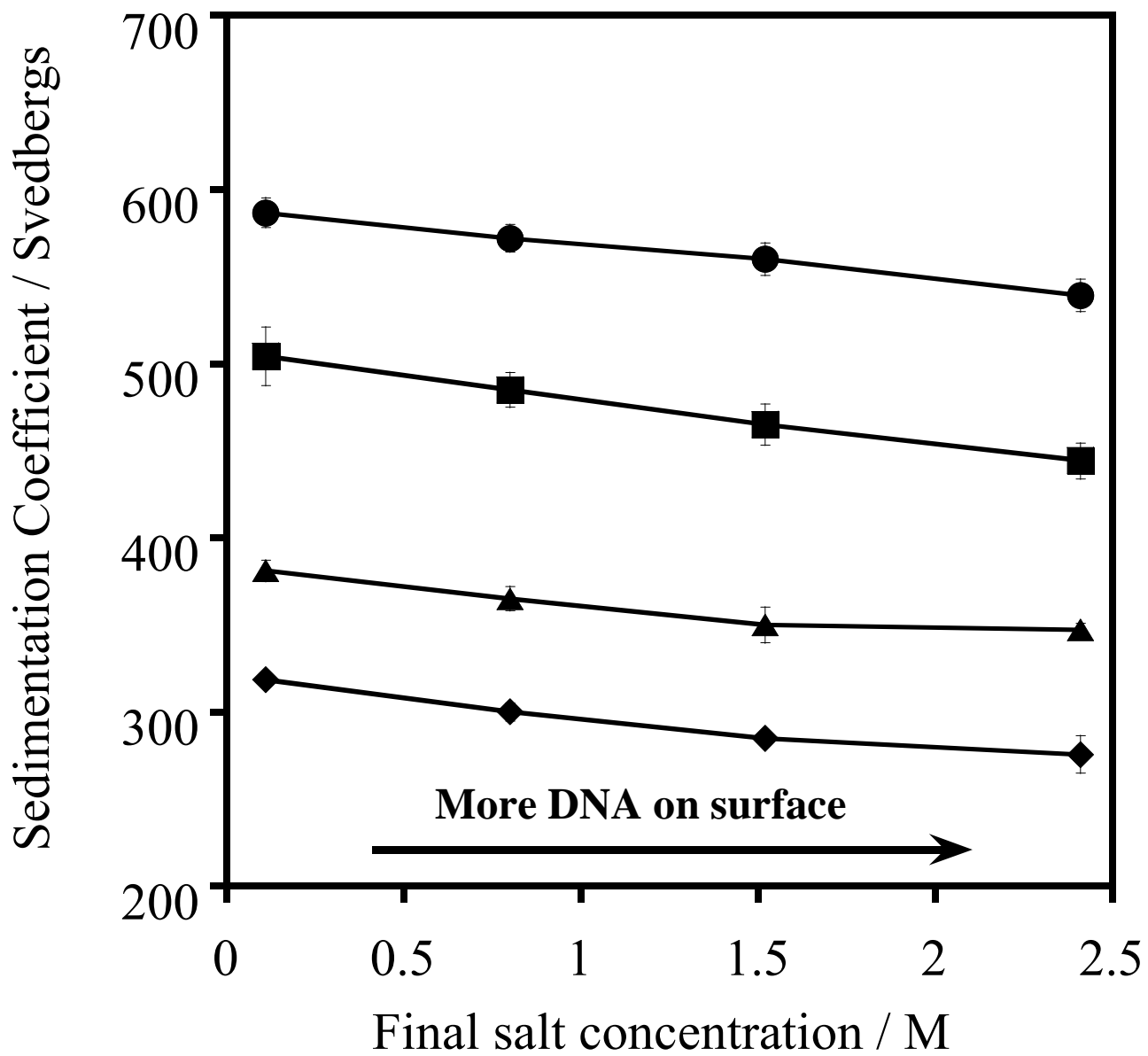


Figure 4. 10 nm gold nanoparticles modified with dT 5 (●), dT 10 (■), dT 20 (▲), dT 30 (◆) sedimented in pure water at $1\,570\text{ rad s}^{-1}$ (15,000 rpm).

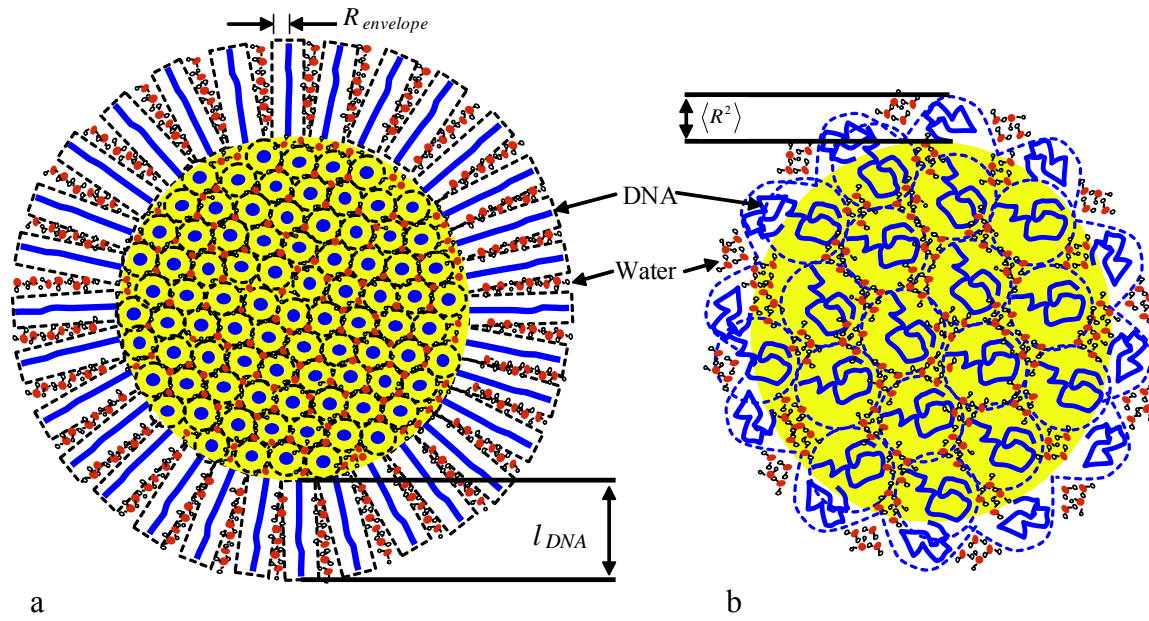


Figure 5. Particle models (a) hydrated fully extended (FE), (b) hydrated worm like chain (WLC).

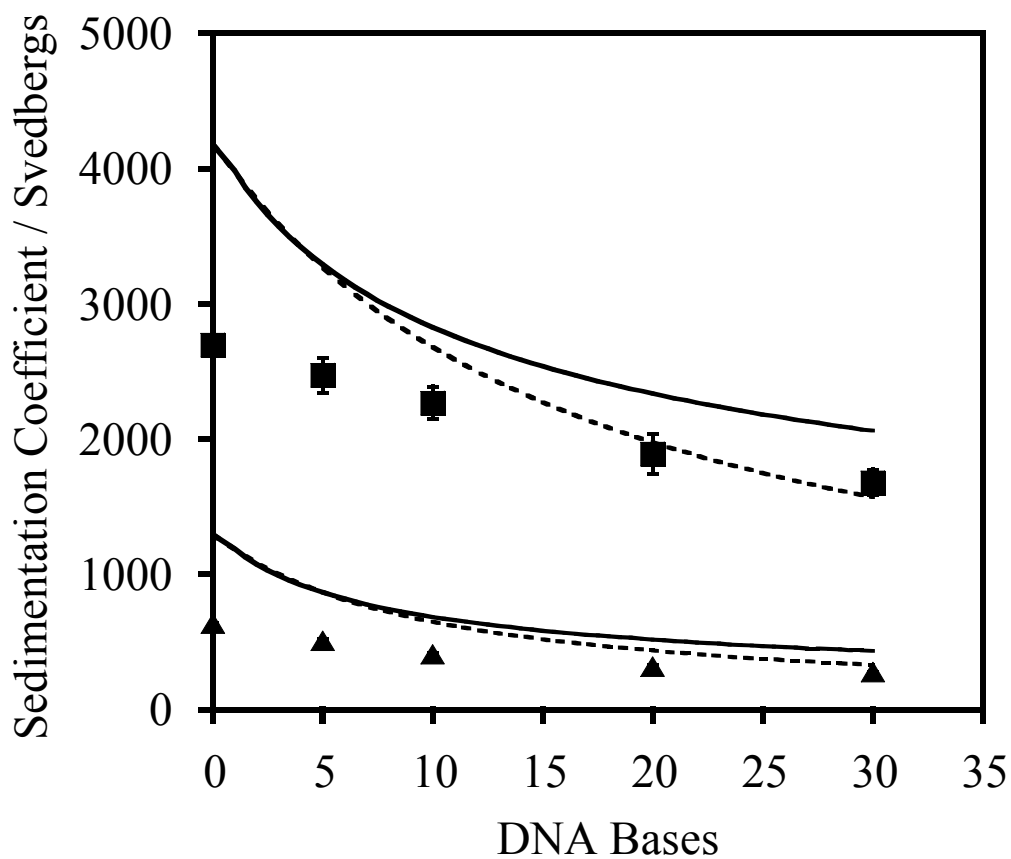


Figure 6. Comparison of (■) WLC and (---) FEC models with measured sedimentation coefficients for (▲) 10 nm and (■) 20 nm diameter gold nanoparticles derivatized with thymidine homooligomers. All sedimentation coefficients were performed in pure water and predictions use a gold particle density of $19\,300\text{ kg m}^{-3}$.

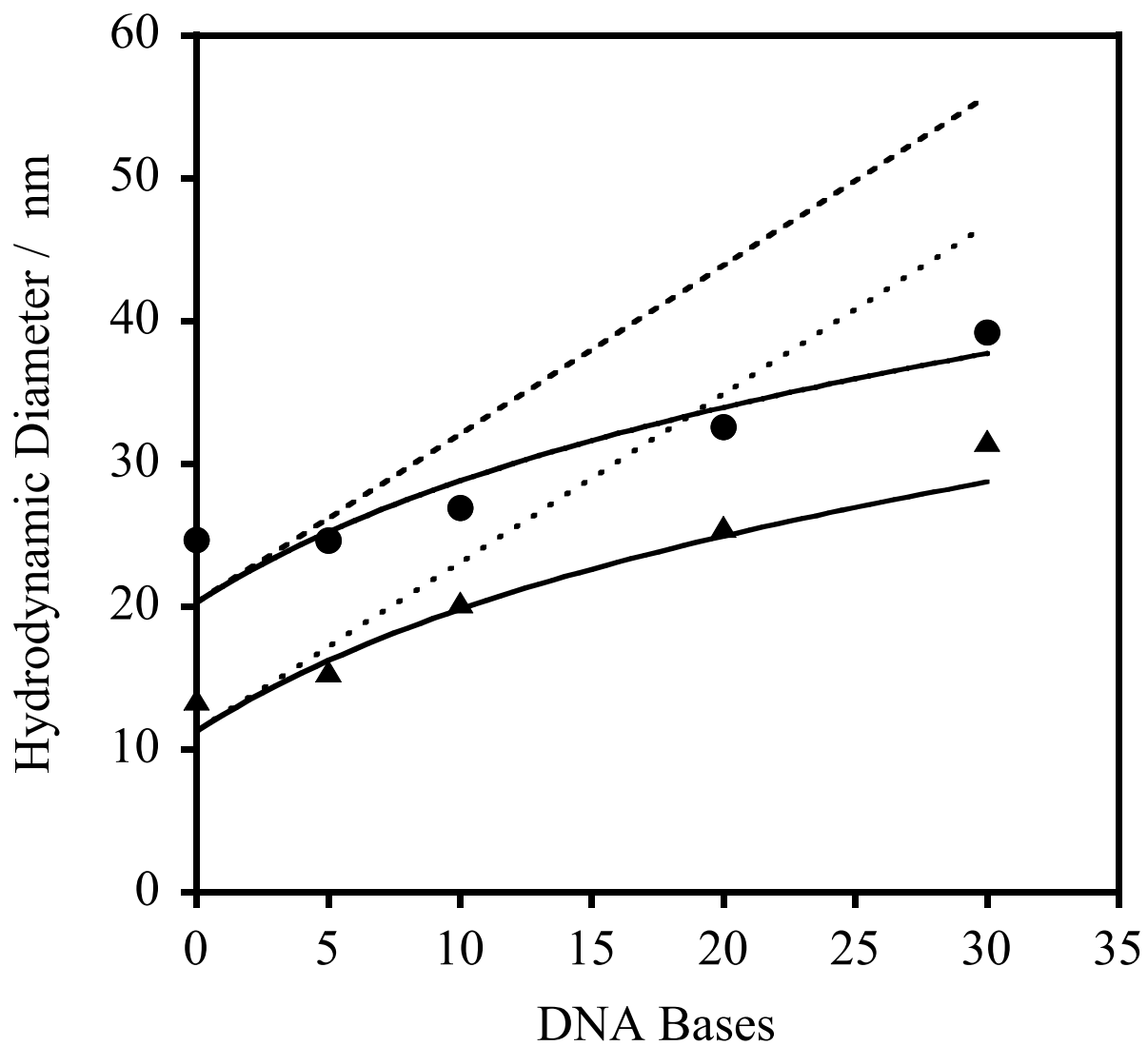


Figure 7. Hydrodynamic diameters measured by dynamic light scattering for thymidine modified (▲) 10 nm gold nanoparticles and (●) 20 nm gold nanoparticles as predicted by the (- -) FE model (-) WLC model.

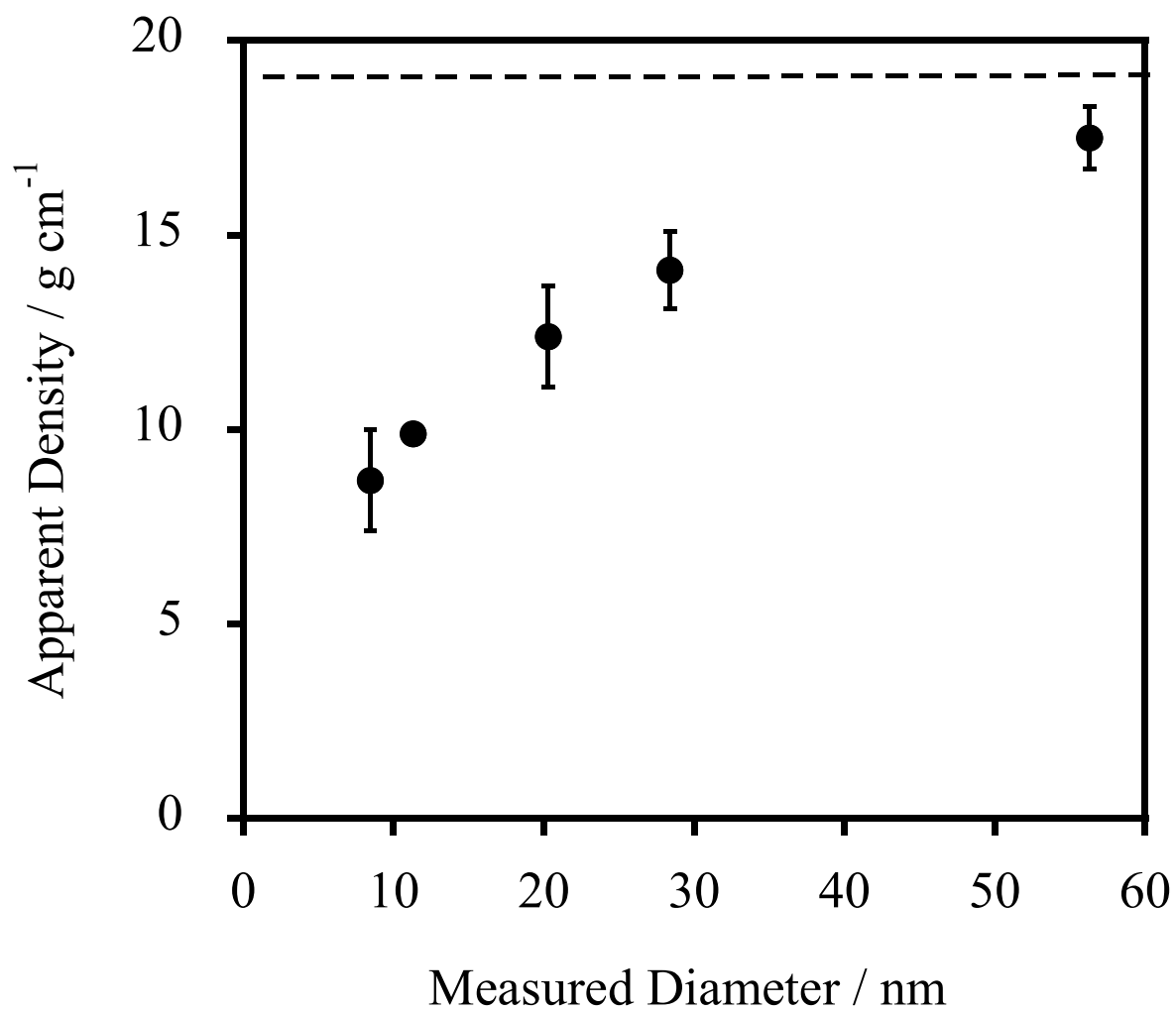


Figure 8. Bare citrate stabilized gold particles sedimented in deionized water. The dashed line marks the density of bulk gold $19\,300\text{ kg m}^{-3}$.